Spectroscopy of methylcyanodiacetylene revisited. Solid parahydrogen and solid neon matrix studies

U. Szczepaniak, A. Gutiérrez-Quintanilla, Claudine Crépin, J.-C. Guillemin, M. Turowski, T. Custer, R. Kolos

Journal of Molecular Structure 1218 (2020) 128437

Contents lists available at ScienceDirect

Journal of Molecular Structure

journal homepage: http://www.elsevier.com/locate/molstruc

Spectroscopy of methylcyanodiacetylene revisited. Solid parahydrogen and solid neon matrix studies

Urszula Szczepaniak [a, b, 1], Alejandro Gutiérrez-Quintanilla [a, c, 2], Claudine Crépin [a, **], Jean-Claude Guillemin [d], Michał Turowski [b], Thomas Custer [b], Robert Kołos [b, *]

[a] Université Paris-Saclay, CNRS, Institut des Sciences Moléculaires d'Orsay, 91405, Orsay, France
[b] Institute of Physical Chemistry, Polish Academy of Sciences, Kasprzaka 44/52, 01-224, Warsaw, Poland
[c] Instituto Superior de Tecnologías y Ciencias Aplicadas (InSTEC), Universidad de La Habana. Ave. Salvador Allende No. 1110, Quinta de los Molinos, La Habana, 10400, Cuba
[d] Univ Rennes, Ecole Nationale Supérieure de Chimie de Rennes, CNRS, ISCR-UMR 6226, F-35000, Rennes, France

ARTICLE INFO

Article history:
Received 23 April 2020
Accepted 11 May 2020
Available online 18 May 2020

Keywords:
Matrix isolation
IR spectroscopy
UV/Vis spectroscopy
Phosphorescence
Polyyne

ABSTRACT

Electronic phosphorescence and infrared absorption spectra of methylcyanodiacetylene (CH_3C_5N) are revisited using matrix isolation in solid parahydrogen and neon. Band assignments previously found for Ar, Kr, Xe, and N_2 low-temperature host media were updated, with certain ambiguous attributions being resolved. A combined analysis of both dispersed phosphorescence and phosphorescence excitation spectra observed in different environments provides a means to estimate the singlet-triplet separation for the gas-phase and pure solid compound, where phosphorescence could not be observed.

1. Introduction

$CH_3(C{\equiv}C)_nCN$ nitriles are of astrochemical importance. The n = 0, 1, and 2 molecules have already been confirmed in the interstellar medium [1–8] and the presence of species with larger n has been postulated (*e.g.* Ref. [9–12]). Acetonitrile and methylcyanoacetylene have also been found in Titan's atmosphere [13,14].

Methylcyanodiacetylene, CH_3C_5N (methylcyanobutadiyne, 2,4-hexadiynenitrile, 1-cyano-2,4-pentadiyne), was first detected in the Taurus Molecular Cloud [7]. In space, it is probably synthesized from HC_5N through a reaction with $CH_3OH_2^+$ [15]. In the laboratory, the molecule has been produced through photolysis of small gaseous acetylenic derivatives of significance to planetology or astrochemistry [16].

Theoretical studies [9,17–19] have provided MP2, DFT or CCSD(T) predictions for a variety of parameters of CH_3C_5N including its molecular geometry, rotational constants, electric dipole moment and polarizability. Laboratory gas-phase microwave [20,21] and infrared [19] transitions have been measured. We described the vibrational (Szczepaniak et al. [22], hereafter: Paper I) and electronic (Turowski et al. [23], hereafter: Paper II) spectroscopy both of the pure solid and of CH_3C_5N isolated in various inert cryogenic matrices. Although much is known, certain problems with spectral analyses persist, including the identification of the ν_8 vibrational mode, interpretation of the ν_2/ν_3 region in the IR, and the weakness of the observed electronic absorption that prohibited any detailed vibronic analysis.

This study aims to bridge these gaps through use of the previously unexplored cryogenic hosts parahydrogen (p-H_2) and Ne. The study was accompanied by sensitive detection of phosphorescence enabled by highly selective tuneable UV laser electronic excitation. Parahydrogen has unique properties [24] that can help in resolving spectroscopic ambiguities observed in other media. On one hand, matrix site effects (*i.e.* frequency shifts due to slightly different microenvironments) are reduced in p-H_2; guest molecules usually occupy only one kind of site, simplifying the spectroscopy. On the other hand, motions such as rotation around a methyl group axis are only weakly perturbed in that solid host [25,26]. Solid neon is

* Corresponding author.
** Corresponding author.
E-mail addresses: claudine.crepin-gilbert@universite-paris-saclay.fr (C. Crépin), rkolos@ichf.edu.pl (R. Kołos).
[1] *Present address: IRsweep AG, Laubisruetistrasse 44, 8712 Staefa, Switzerland.*
[2] *Present address: Aix-Marseille Université, Laboratoire PIIM, Team ASTRO, Service 252, Saint Jérôme, Ave. Escadrille Normandie Niemen, 13013 Marseille, France.*

https://doi.org/10.1016/j.molstruc.2020.128437

also useful as it produces the smallest gas-to-matrix frequency shifts of the rare gas solids and also compared with solid parahydrogen. While phosphorescence of gaseous samples is inherently difficult to detect, measuring spin-forbidden transition frequencies in various cryogenic matrices provides useful estimations of the gas-phase values.

2. Experimental Details

CH_3C_5N was synthesized following the method developed by Kerisit et al. [16,27]. The compound was refined by pumping out CO_2 and other volatile impurities at approx. 200 K, directly before the experiments. The procedure applied for p-H_2 samples was reported by Gutiérrez-Quintanilla et al. [26,28,29]. Briefly, normal hydrogen (5.5, Air Liquide) is converted into its pure *para* form over a catalyst (Fe_2O_3 powder) at around 16 K, within a *Displex* DE202FF or DE202S cryostat. The CH_3C_5N vapour flux (supplied from a tube containing the crystalline substance maintained at 210−250 K) and that of parahydrogen were regulated with needle valves. The resultant mixture solidified on a diamond substrate window held at 3 K (as measured and regulated with a Cryo-con temperature controller) within a closed-cycle helium refrigerator ICES3731 (ICEoxford Ltd.) equipped with external CaF_2 windows. The same cryostat was used for Ne (5.0, Messer) matrices. In the latter case, a gas mixture CH_3C_5N/Ne of 1/1000 was slowly deposited onto a cold window. The composition of the samples was verified with a Nicolet *Nexus* 670/870 FTIR spectrometer with a maximum resolution of 0.125 cm^{-1} and equipped with a liquid nitrogen-cooled MCT detector. Spectra were derived from at least 512 averaged interferograms.

Selectively excited phosphorescence provided insight into the electronic spectroscopy of CH_3C_5N. The basic measurement involves excitation at a fixed wavelength followed by the detection of a dispersed emission spectrum. Alternatively, the excitation wavelength could be changed systematically with predefined steps while the phosphorescence signal was recorded. A Continuum Surelite II + OPO Horizon laser system, operating with a pulse repetition rate of 10 Hz, served as the excitation source between 192 and 400 nm. Phosphorescence was dispersed with an Acton SpectraPro 2300i (Princeton Instruments) grating monochromator (0.3 m, 1200 grooves/mm, resolution of ~0.08 nm) and detected by a CCD camera (Andor *iStar* DH720) sensitive up to 800 nm. A homemade triggering device provided synchronization of the time-gated signal acquisition for a train of laser pulses.

Phosphorescence decay time measurements were carried out using a 0.6 m Jobin-Yvon grating monochromator and a Hamamatsu H3177-50 PMT photomultiplier controlled by a PCIe-6251 card (National Instruments) using custom Labview programs.

3. Results and discussion

3.1. IR absorption

Paper I described several challenges associated with the assignments of IR bands. One of these concerned the ν_2, ν_3 region. In solid nitrogen, the weakest (and lowest wavenumber) of the three bands observed in that area shows the same doublet substructure (probably coming from a site-splitting) as the mid-intensity band, suggesting a common origin of the two. For Ne and p-H_2 hosts, the splitting patterns of thus far unknown provenance appear exclusively for the weakest band (ν_3, see Fig. 1). The middle band, most likely originating in a combination mode, may gain intensity from anharmonic interaction with ν_2 and/or ν_3. The pertinent combination is presumably $\nu_5+\nu_7$, rather than $\nu_6+\nu_7$ suggested in Paper I. The $\nu_6+\nu_7$ has been re-assigned to a band at ~2180 cm^{-1}.

Substructures in IR bands of parahydrogen-isolated molecules appear especially for perpendicular (e ← a_1) transitions ν_9, ν_{10}, and ν_{11}. This is depicted in Fig. 2 for the ν_{10} mode, while unabridged IR spectra S1 and S2 in the Supplementary Information (SI) show the regions of ν_9 and ν_{11}. The said structures seem related to rovibrational features of the respective gas-phase bands, reported in Paper I. In frozen p-H_2, the end-to-end rotation is blocked but the methyl rotation can be only slightly hindered. It allows to consider a rotational constant A associated with the main molecular axis and it

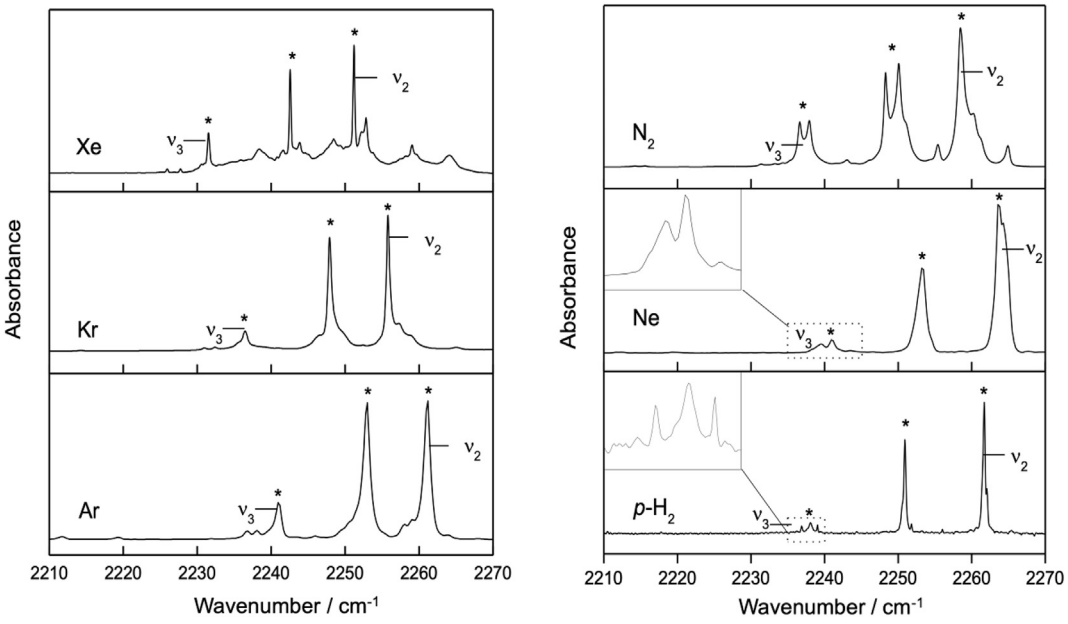

Fig. 1. The ν_2, ν_3 region in IR absorption of CH_3C_5N in various cryogenic hosts: Xe, Kr, N_2 (as reported in Paper I; spectral resolution of 0.16 cm^{-1}), Ar (Paper I, resolution 0.5 cm^{-1}), Ne (this work, resolution 0.5 cm^{-1}) and p-H_2 (this work, resolution 0.125 cm^{-1}). Asterisks mark three bands presumably coupled by an anharmonic interaction (the middle one may represent $\nu_5+\nu_7$). Arbitrary absorbance scales.

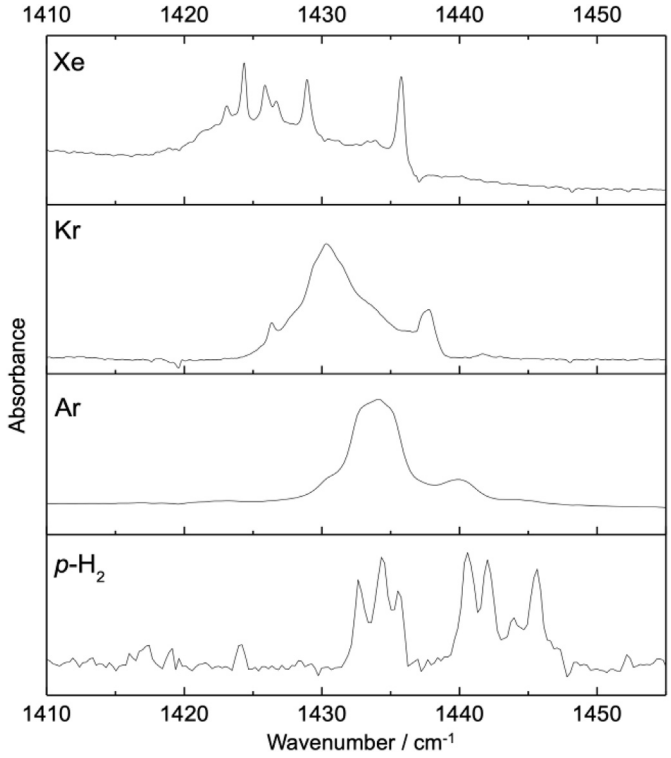

Fig. 2. Spectral region of the vibrational mode ν_{10} for CH_3C_5N isolated in several cryogenic matrices. Distinct substructures are observed in Xe and p-H_2.

may lead to a structure in perpendicular bands involving different K numbers. This case is fully described by Lee et al. [25] for p-H_2-isolated CH_3F. Analogous structures in parallel and perpendicular bands were recently detected for another C_{3v} molecule, propyne, isolated in p-H_2 [28]. Studies are under way to quantify this phenomenon, further complicated by the presence of residual *ortho*-H_2 species, susceptible to clustering around target molecules. That last effect may induce some additional substructure of a vibrational band, as demonstrated in the study of CH_3F [25,30]. There is some similarity between the rotation-related spectral features of CH_3C_5N in p-H_2 and the multiplets observed for the Xe-isolated compound (Fig. 2). It is currently difficult to conclude on either site-splitting origin or rovibrational origin of these latter (similar to the features of acetonitrile in solid Xe [31]).

Table 1 provides collective information on the measured fundamental vibrations. Paper I gave a tentative identification of the weak feature adjacent to the ν_{12} band in argon, assigning it to the C—C stretching mode ν_8. This earlier attribution does not seem likely, as the feature did not appear in any of the other cryogenic solids nor in the gas phase. Neither could it be inferred from the vibronic structure of phosphorescence (see *Electronic spectroscopy* section).

The identified combination and overtone IR bands are listed in Table 2 for each of the hosts tested. In Ne and p-H_2, the CH_3C_5N concentration was too small to enable the measurement of the weaker bands. Additionally, IR absorption by p-H_2 prevents any spectral measurements around 4500 cm^{-1}.

The comparison of diverse environments (Tables 1 and 2), points to vibrational frequency shifts that surpass those anticipated from the varying polarizability of host species. In particular, the locations of certain IR bands in Ar differ notably from those that could be interpolated based on the measurements of other matrices and on the respective polarizability values (see the plots presented in Fig. S3 (SI)).

Spectral attributions given in Table 2 include several improvements, compared to those of Paper I. These regard, in particular, $\nu_6 + \nu_7$, $\nu_5 + \nu_7$, and the replacement of contributions from ν_8 with those from ν_{12}.

3.2. Electronic spectroscopy

Basic knowledge concerning the electronic energy levels of CH_3C_5N is summarized in Table 3. The investigated systems include $\tilde{A}\ ^1A_2 - \tilde{X}\ ^1A_1$ (formally forbidden due to orbital symmetry reasons), $\tilde{B}\ ^1E - \tilde{X}\ ^1A_1$ (formally allowed but observed only when coupled with an e-symmetry vibration), and the spin-forbidden $\tilde{a}\ ^3A' - \tilde{X}\ ^1A_1$.

Analysis of $\tilde{a}$-$\tilde{X}$ phosphorescence relied on emission spectra (see Figs. 3 and 4) excited at the wavelength of a strong absorption band (12_0^1) of the $\tilde{B} - \tilde{X}$ system. Phosphorescence is dominated by a

Table 1
Wavenumber values (cm^{-1}) of fundamental vibrational bands, as measured in IR absorption spectra of CH_3C_5N.

Mode	Cryogenic matrices						Gas phase [a]
	Ne	p-H_2	Ar [a]	N_2	Kr	Xe	
a_1 symmetry							
ν_1	2940, 2947.2	2930	2930.9, 2932.4	2931.2, 2933.5	2919.6, 2920.8	2909–2917	2932.2 (P), 2939.4 (R)
ν_2 [b]	2263.8	2261.6	2261.2	2258.5	2255.8	2251.2	2265
ν_3 [b]	2241, 2239.5	2238.0	2240.9	2236.6, 2237.9	2236.5	2231.5	2246
ν_4	2123.2	2121.4	2121.8	2119	2117.3	2113.2	2118 (P), 2123 (R)
ν_5	1383	1380	1377.6	1380.4	1376.4	1373.1	1379.5
ν_6	–	–	1280.4	1276.3	1277.3	1274.8	1282.1
ν_7	–	–	913.0	910.6	910.5	908	908 (P), 913.3 (R)
ν_8	–	–	–	–	–	–	–
e symmetry							
ν_9	2985.5	2983-2986 [c]	2982.1	2982.2, 2981.1, 2980.3	~2970	2960.4, 2958.2, 2956.5	2982.4 ± 0.1 [e]
ν_{10}	1441	1433-1446 [d]	1434.0	1434.6	1430.5	~1420–1435 [d]	1443 ± 0.3 [e]
ν_{11}	1027	1025.6	1022.5	1023	1021	1019.8	1027.56 ± 0.05 [e]
ν_{12}	–	–	498.6	499.5, 500.3	497.9	496.4, 497.3	500.0
ν_{13}	–	–	465.8	466.4	465.6	464.5	463.4

[a] As reported in Paper I; (P) and (R) refer to rotational branches.
[b] Bands in anharmonic interaction (see text).
[c] Broad.
[d] A well-defined multiplet.
[e] Estimated band origin, indicated by rovibrational branches.

Table 2
Wavenumber values (cm^{-1}) for the identified combination and overtone vibrational modes of CH_3C_5N isolated in cryogenic host solids.

Mode[a]	Ne	*p*-H_2	Ar[b]	N_2	Kr	Xe
$\nu_{12}+\nu_{14}$	–	–	797.1[c]	800.9	796.5	794.1
$2\nu_{13}$	–	–	934.5	935.3, 937.0	934.1	931.6
$\nu_{11}+\nu_{15}$	–	–	1221.5	1234.3	–	–
$\nu_{11}+\nu_{14}$	1357, 1360.5	1354.6	1354	1358.2[d]	1351.7	1341.8[d]
$2\nu_{11}$	2044.4	2039.6	2035.1	2037.9, 2032.9	2030.8	2027.8
$\nu_6+\nu_7$	2180.4	2180.5	2185.3	2179.7	2179.8	2175
$\nu_5+\nu_7$	2253.3	2250.9	2253.0	2250.1, 2248.3	2247.9	2242.6
$\nu_5+\nu_{11}$	~2290	2286.4	2288.9	2287.4[d]	2283.7?	2278.8?
$\nu_{10}+\nu_{11}$	2466.8	2462	2454.8	2458.2, 2455.4	2450.8	2443.5, 2444.9, 2447
$2\nu_6$	2547.4, 2548.8	2551.3	2559.1	2551.1, 2550.2	2553.1	2547.9
$\nu_5+\nu_6$	2656.3	2654.7	2656.2	2654.7, 2652	2650.6	2646.1
$2\nu_5$	2729[e]	2725.5	~2725	~2727, 2706.1[d]	2720.3	2714.8
$\nu_3+\nu_{12}$ *	2737.4	2742.7	2738.8	~2737	2733.4	2727.7
$\nu_5+\nu_7+\nu_{12}$ *	2750.3	2748.8	2753.7	2748.7, 2747.3	2746.5	2739.2
$\nu_2+\nu_{12}$ *	2763.1	2760.9	2763.4	2759.2	2756	2749.3
$2\nu_{10}$	2862.6, 2865.8	2854.2	2848.7	2848.8	2841.7	2835.4
$\nu_4+\nu_7$	3027.1	3024	3028.2	3023.3, 3022.1	3021.3	3014.4
$\nu_5+2\nu_7$	3146.2	3141.8	3146.2	3143.4, 3141.2	3140.3	3132
$\nu_2+\nu_7$	3159.9	3157.1	3160.2	3155.6, 3153.3	3152.8	3145.2
$\nu_2+2\nu_{13}$	–	3191	3185.5	–	–	–
$\nu_5+\nu_7+2\nu_{12}$	–	–	3196.3	–	–	–
$\nu_2+2\nu_{12}$	–	–	3204.1	3202.6, 3200.3	3197.8	–
$\nu_4+\nu_6$	3391.5, 3393.3	3392.5	3397.5	3390.3, 3389.3	3389.8	3382.9
$\nu_1+\nu_{11}$	–	–	3945.4	–	–	–
$2\nu_4$	4237	4234.2	4235.3	4229.2, 4228.2	4225.9	4217.7
$\nu_5+\nu_9$	~4370	–	4349.2	4357.4	–	–
$\nu_9+\nu_{10}$	~4415	–	4400.9	~4405	~4387[d]	4372.2
$2\nu_3$ *	–	–	4481.9	4475.8	–	4462.9
$\nu_2+\nu_3/\nu_2+\nu_5+\nu_7$ *	–	–	4504.6	~4499	–	4485
$2\nu_2$ *	~4512[d]	–	4521.5	~4517	~4494[d]	4502.2

[a] Modes marked with * produce triplets similar to that observed around 2250 cm^{-1}.
[b] As reported in Paper I.
[c] Not reported in Paper I.
[d] Broad and/or weak, wavenumber less certain.
[e] Tentative.

Table 3
Energy (eV) of vibrationless electronic transitions between the ground and selected excited electronic states of CH_3C_5N.

State	This work		Paper II				
	Ne	*p*-H_2	Ar	N_2	Kr	Xe	Gas phase
$\tilde{A}\ ^1A_2$ [a]	4.01	3.97	3.93	3.95	3.91	3.89	4.03
$\tilde{B}\ ^1E$	4.31[b]	4.27[b]	4.23[b]	4.24[b]	4.21[b]	4.19[b]	4.33
$\tilde{a}\ ^3A'$	2.98	2.96	2.94	2.94	2.92	2.92	–

[a] Based on a theoretically predicted value of ν_{12} (Paper II); the estimated error is ±0.03 eV.
[b] Based on the gas-phase value of ν_{12} (Paper II).

vibronic progression in the ν_2 mode (see Fig. 3). Some $\tilde{a}$-$\tilde{X}$ features of the important region between the system origin and 2_1^0 are shown in Fig. 4, together with their spectral assignments. Vibronic bands measured in Ne and *p*-H_2 matrices generally exhibit intensity patterns similar to those observed in Kr, Xe, and N_2. As pointed out in Paper II, the Ar host tends to amplify the $2_n^0 12_1^0$ bands with respect to other $2_n^0 b_1^0$ combinations (b standing for a bending mode), reminiscent of what was found [32] for the mode ν_8 of HC_5N (a zig-zag bending related to ν_{12} of CH_3C_5N).

Compared to the attributions reported in Paper II, several changes are proposed (see Table 4 and the complete listing in Table S1 of SI) based on new data from Ne and *p*-H_2 matrices, re-examination of spectra previously acquired for Ar, Kr, Xe, and N_2 hosts, and an improved wavelength calibration of the Ar-matrix spectra reported in Paper I. Krypton and *p*-H_2 environments usually offered the best resolution of vibronic features.

New assignments of the modes previously identified as ν_5 and

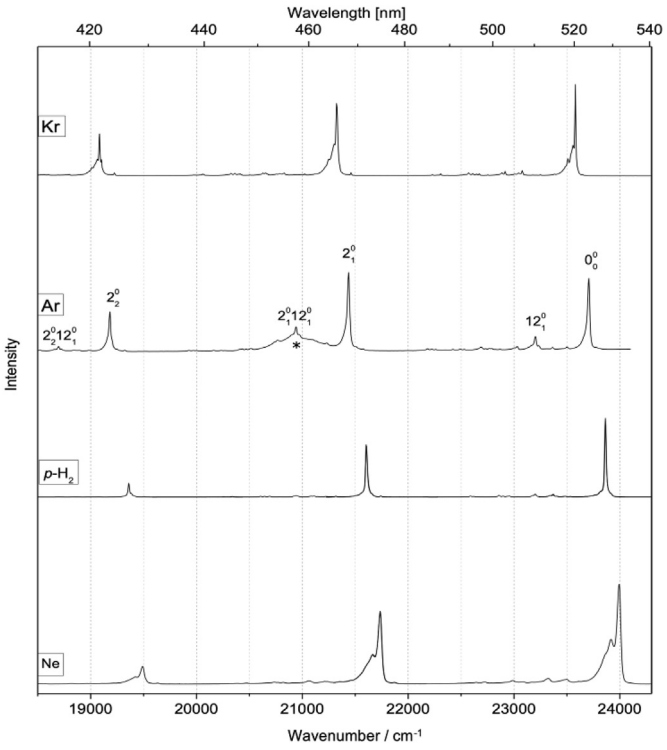

Fig. 3. Phosphorescence of matrix-isolated CH_3C_5N, excited via 12_0^1 $\tilde{B}$-$\tilde{X}$ transition. Vibronic assignments are given for the most intense bands observed in solid Ar, as identified in Paper II. The broad feature marked with an asterisk in the Ar-matrix spectrum is an instrumental artifact.

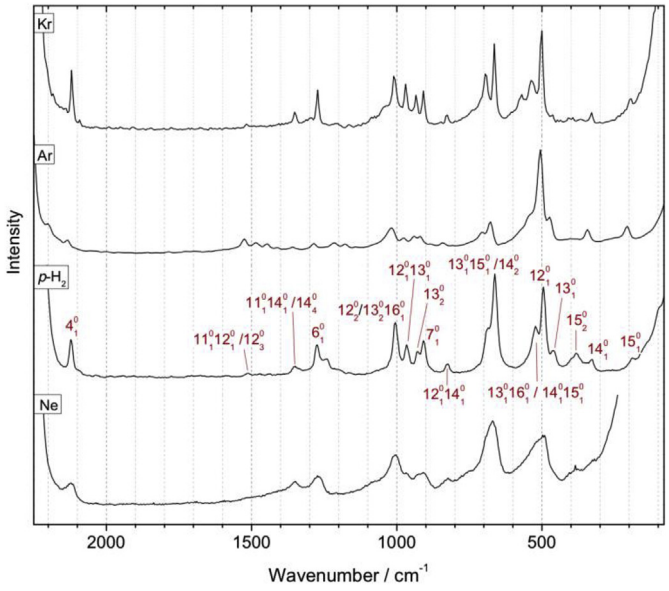

Fig. 4. CH_3C_5N phosphorescence in various matrices. Spectra aligned with respect to their vibrationless origins (23 995 cm^{-1} in Ne, 23 863 cm^{-1} in p-H_2, 23 708 cm^{-1} in Ar, 23 580 cm^{-1} in Kr), arbitrarily located at 0 cm^{-1}.

ν_{11}, as well as several combination bands involving these fundamentals, were prompted by a substantial mismatch between fundamental frequencies derived from phosphorescence spectra and those taken from vibrational spectroscopy data. Several new attributions of combination modes are made using analogies to HC_5N spectroscopy and from the assumption that anharmonicity is similar for alike bending modes. For example, in the case of a zig-zag deformation ν_{12} (498 cm^{-1} in Kr), the anharmonicity is assumed to be negligible, just as it is for the analogous mode ν_8 of HC_5N (the latter is observed [32] in Kr at 506 cm^{-1}, with the first overtone at 1011 cm^{-1}). Out of the ν_{13}, ν_{14}, and ν_{15} fundamentals previously detected in Ar, only ν_{14} appeared in Ne (at a relative wavenumber value of 326 cm^{-1}, see Table 4). Based on evidence from this host medium, with no contribution from ν_{13} or ν_{15}, the band at 670 cm^{-1} is more likely due to the $2\nu_{14}$ overtone than to the $\nu_{13} + \nu_{15}$ combination which was previously assigned. The band at ~3511 cm^{-1} is presently identified as $2\nu_6 + 2\nu_{12}$ (see Table S1).

The observed variation of phosphorescence lifetime with changing host media (Table 5) confirms the role of the external heavy atom effect [33] in inducing the spin-orbit coupling. Heavier matrix hosts may amplify both the singlet-triplet intersystem crossing rate and the radiative relaxation of the triplet state.

Phosphorescence excitation spectra of matrix-isolated CH_3C_5N (Fig. 5) are dominated by the $2_0^n 12_0^1$ (n = 0, 1, 2, 3) vibronic progression of the $\tilde{B} - \tilde{X}$ system, which is allowed due to the

Table 4
$\tilde{a} - \tilde{X}$ phosphorescence bands for CH_3C_5N isolated in several cryogenic solids. Relative wavenumber values (cm^{-1}) calculated with respect to vibrationless (*0-0*) $\tilde{a}$-$\tilde{X}$ origins at 23 995 cm^{-1} (Ne), 23 863 cm^{-1} (p-H_2), 23 708 cm^{-1} (Ar) or 23 580 cm^{-1} (Kr).

Relative wavenumber				Intensity[a]	Assignment
Ne	p-H_2	Ar[b]	Kr		
0	0	0	0	vs	0_0^0
–	189	200	196	w	15_1^0
326	330	337	329	w	14_1^0
385	379	–	400	mw	15_2^0
–	461	466	463	mw	13_1^0
498	496	499	500	m	12_1^0
–	522	537[c]	536	mw	$13_1^0 16_1^0$[c] or $14_1^0 15_1^0$
670	663	670	664	m	14_2^0 15_1^0
824	824	833	826	mw	$12_1^0 14_1^0$
910	908	911	908	mw	7_1^0
930	928	932	934	w	13_2^0
968	967	968	970	mw	$12_1^0 13_1^0$
1004	1005	1011	1011	mw	12_2^0[d] or $13_2^0 16_1^0$ [c, e]
1273	1275	1278	1272	mw	6_1^0
1349	1349	1353	1352	w	$11_1^0 14_1^0$ [f] or 14_4^0
–	1513	1517	1518	vw	$11_1^0 12_1^0$ [c] or 12_3^0 [d]
2121	2123	2123	2120	mw	4_1^0
2259	2260	2262	2257	vs	2_1^0
2538	2547	2569	2557	mw	6_2^0
2758	2753	2759	2750	mw	$2_1^0 12_1^0$
2932	2924	2933	2926	mw	$2_1^0 13_1^0 15_1^0$ or 1_1^0 or $2_1^0 14_2^0$
3071	3080	–	3079	vw	$2_1^0 12_1^0 14_1^0$
3176	3173	3185	3167	mw	$2_1^0 7_1^0$
3518	3527	3535	3521	w	$2_1^0 6_1^0$
–	3758	3769	3750	w	$2_1^0 11_1^0 12_1^0$ or $2_1^0 12_3^0$ [d]
4364	4359	4373	4356	mw	$2_1^0 4_1^0$
4504	4503	4514	4496	vs	2_2^0
4781, 4800 [c]	4789	4803	4780	w	$2_1^0 6_2^0$ or $2_2^0 14_1^0$
5030	5026	5040	5021	w	$2_2^0 13_1^0 16_1^0$or $2_2^0 14_1^0 15_1^0$
5176	5161	5174	5154	w	$2_2^0 13_1^0 15_1^0$ or $2_2^0 14_2^0$ or $2_1^0 1_1^0$
5426	5413	5423	5399	w	$2_2^0 13_2^0$or/and $2_2^0 7_1^0$
5745	5742	5771	5749	w	

(*continued on next page*)

Table 4 (*continued*)

Relative wavenumber				Intensity[a]	Assignment
Ne	*p*-H_2	Ar[b]	Kr		
					$2_2^0 6_1^0$
–	6597	–	6572	w	$2_2^0 4_1^0$
6748	6740	–	6713	s	2_3^0
7244	–	–	7238[c]	w	$2_3^0 13_1^0 16_1^0$ or $2_3^0 14_1^0 15_1^0$
–	8957	–	8924	m	2_4^0

[a] May vary, depending on the matrix. Intensity descriptors (s – strong, m – medium, w – weak, v – very) correspond to *p*-H_2. $2_n^0 12_1^0$ bands are stronger in Ar than in other hosts; see Fig. 3.
[b] Values differ from those reported in Paper II, due to improved wavelength calibration of the original spectra.
[c] Tentative.
[d] New interpretation, coming from analogy with HC_5N spectroscopy; see text.
[e] Possible overlap with 11_1^0.
[f] New interpretation, based on IR absorption measurements.

Table 5
CH_3C_5N phosphorescence lifetime, as measured in cryogenic matrices.

Matrix	τ (ms)
Ne	~520 [b]
Ar [a]	~400
N_2 [a]	350
Kr [a]	150
Xe [a]	<1

[a] Ref. 23.
[b] ± 20 ms

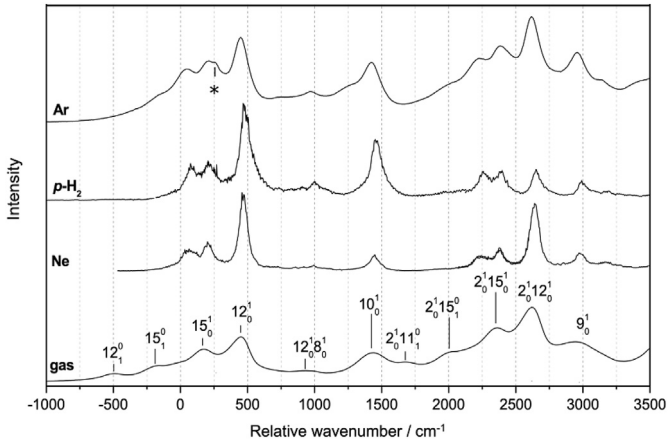

Fig. 5. Phosphorescence excitation spectra of cryogenically isolated CH_3C_5N, juxtaposed with gas-phase electronic absorption. Emission intensity measured at the $\tilde{a}$-$\tilde{X}$ origin. Traces aligned with respect to the origin of $\tilde{B}-\tilde{X}$ (34 925 cm^{-1} in the gas phase [23], 34 715 cm^{-1} in Ne, 34 430 cm^{-1} in *p*-H_2, 34 075 cm^{-1} in Ar [23]), arbitrarily located at 0 cm^{-1}. All labelled bands belong to the $\tilde{B}-\tilde{X}$ system. Asterisk marks an instrumental artifact.

contribution of the ν_{12} bending mode. For the newly measured Ne and *p*-H_2 matrices, the approximate locations of vibrationless origins were obtained making use of the positions of strong 12_0^1 bands and of the measured gas-phase $\tilde{B}$-state ν_{12} frequency (467 cm^{-1}, Paper II). Phosphorescence excitation spectra (contrary to those of dispersed phosphorescence) exhibit similar vibronic patterns in all matrices studied, including Ar (Fig. 5).

As can be seen in the dispersed phosphorescence spectra (Fig. 3), every element of the main (2_n^0) progression within the $\tilde{a}$-$\tilde{X}$ emission in solid neon features a sharp peak and a broad, red-shifted sideband. There is a striking dissimilarity between the phosphorescence excitation spectra (Fig. 6) measured separately for these two components. This difference indicates that the red-shifted sidebands in the dispersed phosphorescence spectra do not originate in phonons or secondary sites; they are most likely due to molecular aggregates.

Weak spectral features due to the $\tilde{A}-\tilde{X}$ system could also be detected and assigned in the phosphorescence excitation spectrum for CH_3C_5N isolated in *p*-H_2 (Fig. 7).

Table 6 lists $\tilde{A}-\tilde{X}$ and $\tilde{B}-\tilde{X}$ bands of CH_3C_5N identified in Ne and *p*-H_2 hosts. The respective Ar-matrix data are included (when available) for comparison. The most important updates with respect to Paper II, include distinguishing a distinct $\tilde{B}-\tilde{X}$ $2_0^n x$ progression (it remains unclear whether "*x*" stands for a phonon or the mode ν_{16}), replacement of the $\tilde{B}-\tilde{X}$ $2_0^n 3_0^1$ attribution with $2_0^n 10_0^1 12_0^1$ and replacement of $\tilde{A}-\tilde{X}$ 11_0^1 with $12_0^1 14_0^2$.

In Fig. 8, wavenumbers of the most intense $\tilde{A}-\tilde{X}$ transition are plotted against those of the most intense $\tilde{B}-\tilde{X}$ feature. In both systems, the strongest band is 12_0^1 (noteworthy, the predicted $\tilde{A}$- and $\tilde{B}$-state ν_{12} frequencies are very similar; see Paper II). The relation is linear, with an intercept of little importance, and

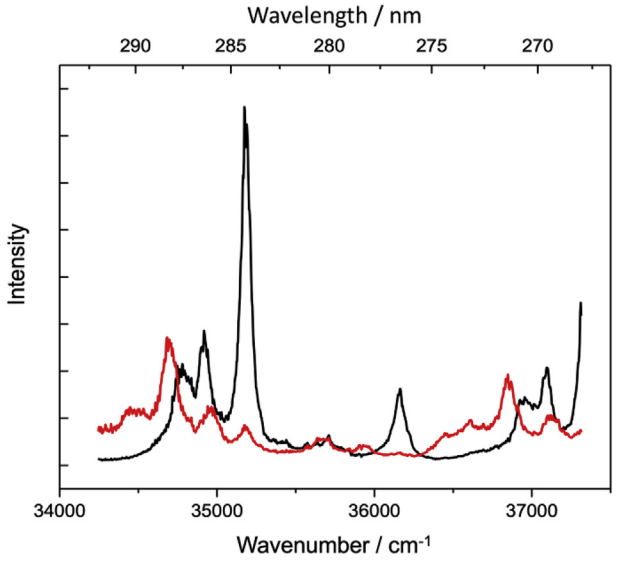

Fig. 6. Phosphorescence excitation spectra for two components of the $\tilde{a}$-$\tilde{X}$ origin (*0-0*) band in solid Ne, detected at 23 995 cm^{-1} (black solid line: isolated CH_3C_5N molecules) and 23 915 cm^{-1} (red solid line: CH_3C_5N aggregates). Ordinate scale is the same for both traces.

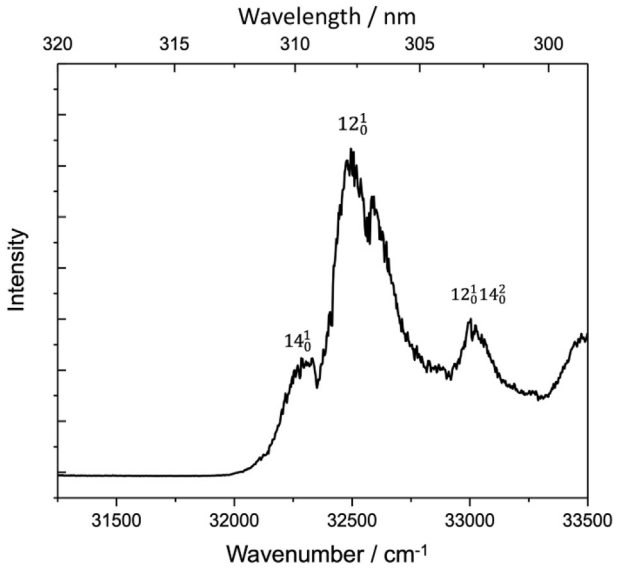

Fig. 7. Phosphorescence excitation spectrum of CH_3C_5N isolated in solid *p*-H_2. Emission detected at 23 863 cm^{-1}. Vibronic assignments refer to the $\tilde{A}-\tilde{X}$ system.

suggests that the $\tilde{A}-\tilde{X}$ origin energy is *ca*. 9% lower than that of $\tilde{B}-\tilde{X}$, irrespective of the environment.

An analogous plot for the $\tilde{a}-\tilde{X}$ origin wavenumbers also shows a linear correlation. While the singlet-triplet separation could not be measured for CH_3C_5N in the gas-phase or pure solid, extrapolation of the bottom line in Fig. 8 hints at a value of 24 100 cm^{-1} (2.99 eV) for the gas-phase and 23 100 cm^{-1} (2.86 eV) for the pure solid.

4. Conclusions

The UV/Vis and IR spectroscopic description of CH_3C_5N was extended based on new *p*-H_2- and Ne-matrix measurements, as well as using additional analyses of the data formerly acquired for diverse host media. All major spectral features have been assigned. Further investigations, involving other simple C_{3v} compounds like propyne, should help to identify the rovibrational features of perpendicular bands observed in IR absorption spectra of *p*-H_2-isolated CH_3C_5N.

The comparison of cryogenic hosts applied for isolating CH_3C_5N

Table 6
Wavenumber values (cm^{-1}) for $\tilde{A}-\tilde{X}$ and $\tilde{B}-\tilde{X}$ systems, as detected in phosphorescence excitation spectra of CH_3C_5N isolated in solid Ne, *p*-H_2, and Ar. Vibronic assignments refer to $\tilde{B}-\tilde{X}$, unless otherwise stated.

Mode	in Ne		in *p*-H_2		in Ar [a]
	absolute	relative to *0-0*	absolute	relative to *0-0*	relative to *0-0*
$\tilde{A}$-$\tilde{X}$ 14_0^1	~32530	−2186	~32300	−2131	
$\tilde{A}$-$\tilde{X}$ 12_0^1	32775	−1941	32495	−1936	−1928
$\tilde{A}$-$\tilde{X}$ $12_0^1 14_0^2$	~33300	−1416	33025	−1406	−1396
phonon	~34785	69	34505	74	62
15_0^1	34921	205	34636	205	231
12_0^1	35183	467	34898	467	467
$12_0^1 15_0^1$ or $13_0^1 14_0^1$	35439	723			752
$8_0^1 12_0^1$	35710	994	35428	997	987
10_0^1	36163	1447	35890	1459	1441
$2_0^1 x$ [b]	~36950	2234	~36690	2259	2242
$2_0^1 15_0^1$	37095	2379	~36815	2384	2399
$2_0^1 12_0^1$	37355	2639	37084	2653	2635
9_0^1	37697	2981	37422	2991	2973
$2_0^1 8_0^1 12_0^1$	~37883	3167	37623	3192	3164
$2_0^1 10_0^1$	38346	3630	38074	3643	3617
$2_0^1 10_0^1 12_0^1$	~38840	4124	~38590	4159	4134
$2_0^2 x$ [b]	~39140	4424	38849	4418	4382
$2_0^2 15_0^1$	39277	4561	38989	4558	4559
$2_0^2 12_0^1$	39526	4810	39239	4808	4801
$2_0^1 9_0^1$	39887	5171	39597	5166	5151
$2_0^2 8_0^1 12_0^1$	40062	5346	39781	5350	5334
$2_0^2 10_0^1$	40525	5809			5789
$2_0^2 10_0^1 12_0^1$	~41030	6314			6307
$2_0^3 x$ [b]	41305	6589			6534
$2_0^3 15_0^1$	41435	6719			6718
$2_0^3 12_0^1$	41679	6963			6950
$2_0^2 9_0^1$	42048	7332			7317
$2_0^3 10_0^1$	~42700	7980			7941
$2_0^3 10_0^1 12_0^1$	43190	8474			8440
$2_0^4 x$ [b]	43475	8759			
$2_0^4 15_0^1$	43614	8898			
$2_0^4 12_0^1$	43825	9119			9088
$2_0^3 9_0^1$	44222	9506			9482
$2_0^4 10_0^1$	44823	10107			
$2_0^4 10_0^1 12_0^1$	45340	10624			
$2_0^5 12_0^1$	45950	11234			
$2_0^4 9_0^1$	46350	11634			
$2_0^5 10_0^1$	46980	12264			

[a] Based on Ref. [23].
[b] A ν_2-governed progression (see text).

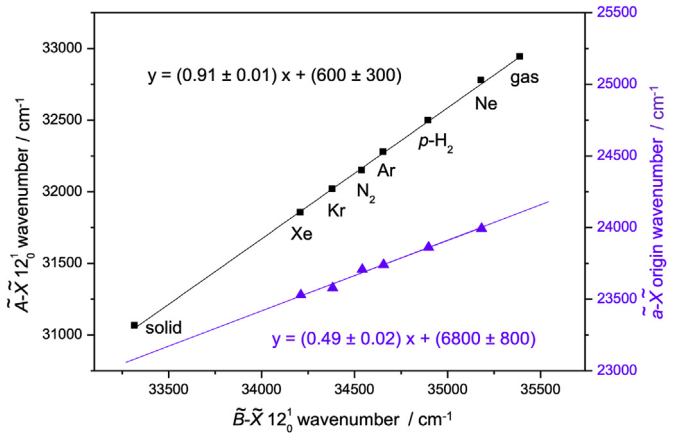

Fig. 8. Dependence of the wavenumber of the most intense bands of $\tilde{A}-\tilde{X}$ (12_0^1; black squares) and $\tilde{a}-\tilde{X}$ (*0-0*; purple triangles) on the wavenumber of the most intense $\tilde{B}-\tilde{X}$ band (12_0^1) of CH_3C_5N. Gas- and solid-phase wavenumbers come from UV–Vis absorption, other values from phosphorescence excitation spectra; data taken in part from Paper II.

revealed subtle peculiarities of phosphorescence observed in solid argon, namely the enhancement of vibronic contributions from certain bending modes. Similar differences were observed in the case of other cyanoalkynes like HC_5N [32] or C_4N_2 [34].

The comprehensive analysis of data acquired for various cryogenic hosts made it possible to estimate the $\tilde{a}-\tilde{X}$ system origin energy both for gas-phase and pure crystalline CH_3C_5N, values which are difficult to obtain directly.

Acknowledgments

This study was supported with the funds of the Polish National Science Centre, project No. 2011/03/B/ST4/02763, the French-Polish PICS project (2014–2016) and the RTRA Triangle de la Physique (2013-0436T REACMAQ). U. Szczepaniak is a beneficiary of the French Government scholarship Bourse Eiffel managed by Campus France. The authors thank Dr. Marcin Gronowski for helpful discussions.

Appendix A. Supplementary data

Supplementary data to this article can be found online at https://doi.org/10.1016/j.molstruc.2020.128437.

References

[1] P.M. Solomon, K.B. Jefferts, A.A. Penzias, R.W. Wilson, Astrophys. J. Lett. 168 (1971) L107–L111.
[2] H.E. Matthews, T.J. Sears, Astrophys. J. Lett. 267 (1983) L53–L57.
[3] P.F. Goldsmith, R. Krotkov, R.L. Snell, R.D. Brown, P. Godfrey, Astrophys. J. 274 (1983) 184–194.
[4] S. Cazaux, A.G.G.M. Tielens, C. Ceccarelli, A. Castets, V. Wakelam, E. Caux, B. Parise, D. Teyssier, Astrophys. J. Lett. 593 (2003) L51–L55.
[5] N.W. Broten, J.M. MacLeod, L.W. Avery, P. Friberg, A. Hjalmarson, B. Hoglund, W.M. Irvine, Astrophys. J. 276 (1984) L25–L29.
[6] L.E. Snyder, T.L. Wilson, C. Henkel, P.R. Jewell, C.M. Walmsley, Bull. AAS 16 (1984) 959.
[7] A. Remijan, J.M. Hollis, L.E. Snyder, P.R. Jewell, F.J. Lovas, Astrophys. J. 643 (2006) L37–L40.
[8] A. Belloche, H.S.P. Müller, K.M. Menten, P. Schilke, C. Comito, Astron. Astrophys. 559 (2013) A47.
[9] E. Herbst, C.M. Leung, Astrophys. J. Suppl. 69 (1989), 271–30.
[10] T.I. Hasegawa, E. Herbst, Mon. Not. Roy. Astron. Soc. 263 (1993) 589–606.
[11] G.E. Hassel, E. Herbst, R.T. Garrod, Astrophys. J. 681 (2008) 1385–1395.
[12] J. Kalvāns, I. Shmeld, Astron. Astrophys. 521 (2010) A37.
[13] V. Vuitton, R.V. Yelle, M.J. McEwan, Icarus 191 (2007) 722742.
[14] J.C. Loison, E. Hébrard, M. Dobrijevic, K.M. Hickson, F. Caralp, V. Hue, G. Gronoff, O. Venot, Y. Bénilan, Icarus 247 (2015) 218–247.
[15] A.J. Markwick, T.J. Millar, S.B. Charnley, Astrophys. J. 535 (2000) 256–265.
[16] N. Kerisit, C. Rouxel, S. Colombel-Rouen, L. Toupet, J.-C. Guillemin, Y. Trolez, J. Org. Chem. 81 (2016) 3560–3567.
[17] V. Moliner, J. Andrés, A. Arnau, E. Silla, I. Tuñón, Chem. Phys. 206 (1996) 57–61.
[18] D.E. Woon, E. Herbst, Astrophys. J. Suppl. 185 (2009) 273–288.
[19] M.M. Montero-Campillo, O. Mó, M. Yáñez, A. Benidar, C. Rouxel, N. Kerisit, Y. Trolez, J.-C. Guillemin, ChemPhysChem 17 (2016) 1018–1024.
[20] A.J. Alexander, H.W. Kroto, M. Maier, D.R.M. Walton, J. Mol. Spectrosc. 70 (1978) 84–94.
[21] W. Chen, J.-U. Grabow, M.J. Travers, M.R. Munrow, S.E. Novick, M.C. McCarthy, P. Thaddeus, J. Mol. Spectrosc. 192 (1998) 1–11.
[22] (Paper 1) U. Szczepaniak, M. Turowski, T. Custer, M. Gronowski, N. Kerisit, Y. Trolez, R. Kołos, ChemPhysChem 17 (2016) 3047–3054.
[23] (Paper II) M. Turowski, U. Szczepaniak, T. Custer, M. Gronowski, R. Kołos, ChemPhysChem 17 (2016) 4068–4078.
[24] M.E. Fajardo, in: L. Khriachtchev (Ed.), Physics and Chemistry at Low Temperatures, Pan Stanford Publishing, Singapore, 2011, pp. 167–202 (and references therein).
[25] Y.-P. Lee, Y.-J. Wu, J.T. Hougen, J. Chem. Phys. 129 (2008) 104502.
[26] A. Gutiérrez-Quintanilla, M. Chevalier, J. Ceponkus, R.R. Lozada-García, J.-M. Mestdagh, C. Crépin, Faraday Discuss 212 (2018) 499–515.
[27] N. Kerisit, L. Toupet, Y. Trolez, J.-C. Guillemin, Chem. Eur J. 19 (2013) 17683–17686.
[28] A.I. Strom, A. Gutiérrez-Quintanilla, M. Chevalier, J. Ceponkus, C. Crépin, T.D. Anderson, Molecules and Complexes with Hydrogen Bond: Solvation and Photoreactivity in Cryogenic Matrices, J. Phys. Chem. A (2016), https://doi.org/10.1021/acs.jpca.0c02900. NNT: 2016SACLS561, Université Paris-Sud/Université Paris-Saclay.
[29] A. Gutiérrez-Quintanilla, M. Chevalier, R. Platakyte, J. Ceponkus, G.A. Rojas-Lorenzo, C. Crépin, Phys. Chem. Chem. Phys. 20 (2018) 12888–12897.
[30] K. Yoshioka, D.T. Anderson, J. Chem. Phys. 119 (2003) 4731–4742.
[31] R. Hattori, E. Suzuki, K. Shimizu, J. Mol. Struct. 750 (2005) 123–134.
[32] M. Turowski, C. Crépin, M. Gronowski, J.-C. Guillemin, A. Coupeaud, I. Couturier-Tamburelli, N. Piétri, R. Kołos, J. Chem. Phys. 133 (2010), 074310.
[33] N. Turro, Modern Molecular Photochemistry, The Benjamin/Cummings Publishing Co., Menlo Park, 1978, p. 124.
[34] M. Turowski, C. Crépin, I. Couturier-Tamburelli, N. Piétri, R. Kołos, Low Temp. Phys. 38 (2012) 723–726.